



# Graphene@hierarchical meso-/microporous carbon for ultrahigh energy density lithium-ion capacitors

Nian-Wu Li <sup>a,b,c,1</sup>, Xinyu Du <sup>a,b,1</sup>, Ji-Lei Shi <sup>c,1</sup>, Xiuling Zhang <sup>a,b</sup>, Wei Fan <sup>a,b</sup>, Jiaona Wang <sup>d</sup>, Shuyu Zhao <sup>a,b,d</sup>, Yuebo Liu <sup>d</sup>, Weihua Xu <sup>a,b,\*\*</sup>, Meicheng Li <sup>e</sup>, Yu-Guo Guo <sup>c,\*\*\*</sup>, Congju Li <sup>a,b,\*</sup>

<sup>a</sup> Beijing Institute of Nanoenergy and Nanosystems, Chinese Academy of Sciences, Beijing, 100083, PR China

<sup>b</sup> School of Nanoscience and Technology, University of Chinese Academy of Sciences, Beijing, 100049, PR China

<sup>c</sup> CAS Key Laboratory of Molecular Nanostructure and Nanotechnology, CAS Research/Education Center for Excellence in Molecular Sciences, Institute of Chemistry, Chinese Academy of Sciences (CAS), Beijing, 100190, PR China

<sup>d</sup> School of Materials Science & Engineering, Beijing Institute of Fashion Technology, Beijing, 100029, PR China

<sup>e</sup> State Key Laboratory of Alternate Electrical Power System with Renewable Energy Sources, School of Renewable Energy, North China Electric Power University, Beijing, 102206, PR China



## ARTICLE INFO

### Article history:

Received 15 March 2018

Received in revised form

13 May 2018

Accepted 23 May 2018

Available online 24 May 2018

### Keywords:

Graphene

Meso-/microporous carbon

Lithium-ion capacitor

Interface adsorption

## ABSTRACT

Li-ion capacitors (LICs) are promising devices to realize the high energy density at high power density. Unfortunately, the development of high energy density LICs is hindered by the low capacity of capacitor-type cathode. Herein, we design a graphene@hierarchical meso-/microporous carbon (G@HMMC) with rational oxygen containing group for ultrahigh energy density LICs. In the ingenious designed G@HMMC material, the novel hierarchical meso-/microporous carbon provides abundant adsorption sites, the graphene structure provides high-speed channel for electron, and rational oxygen-containing group enhances the specific capacity. Therefore, the ingenious designed lithium-ion capacitor composed of G@HMMC cathode and pre-lithiated graphite anode demonstrates ultrahigh energy densities of 233.3–143.8 Wh kg<sup>-1</sup> at power densities from 450.4 to 15686 W kg<sup>-1</sup>. Consequently, the G@HMMC material is one of the most promising cathode materials for LICs. The simultaneous manipulation of hierarchical meso-/microporous structure, sp<sup>2</sup> type carbon, and oxygen-containing group provides new opportunities for the high-performance electrodes.

© 2018 Published by Elsevier Ltd.

## 1. Introduction

Advanced energy-storage systems with various characteristics, including high energy density, high power density, and long cycling life are needed to satisfy the increasing development of electrical transportation, consumer electronics, clean energy storage, and grid storage [1–5]. Lithium-ion batteries (LIBs) and electrochemical

supercapacitors (ECs) are the most promising devices among these energy-storage systems. LIBs deliver a specific energy of 150–250 Wh kg<sup>-1</sup>, but with low power density (<400 W kg<sup>-1</sup>). While ECs possess high power density of 10 kW kg<sup>-1</sup>, but with specific energy density of less than 10 Wh kg<sup>-1</sup> [6–14]. Special energy-storage devices with high energy density and power density are highly desired. As a result, a hybrid energy-storage device inheriting the individual advantages of LIBs and ECs is designed by integrating the working mechanism of LIBs and ECs [15,16]. The new designed lithium-ion capacitors (LICs) are generally composed of a capacitor-type cathode with fast charge/discharge capability and a battery-type anode with large capacity [17–21]. However, the development of LICs with high energy density and power density is hindered by the mismatch of charge-storage capacity and electrode kinetics between capacitor-type cathode and battery anode. To address the sluggish kinetics of battery-type anode, many fast and large capacity anodes were developed for LICs [22–27]. Therefore,

\* Corresponding author. Beijing Institute of Nanoenergy and Nanosystems, Chinese Academy of Sciences, Beijing, 100083, PR China.

\*\* Corresponding author. Beijing Institute of Nanoenergy and Nanosystems, Chinese Academy of Sciences, Beijing 100083, PR China.

\*\*\* Corresponding author. Institute of Chemistry, Chinese Academy of Sciences, 100190, PR China.

E-mail addresses: [whxu@genetics.ac.cn](mailto:whxu@genetics.ac.cn) (W. Xu), [yguo@iccas.ac.cn](mailto:yguo@iccas.ac.cn) (Y.-G. Guo), [licongju@binn.cas.cn](mailto:licongju@binn.cas.cn) (C. Li).

<sup>1</sup> These authors contribute equally to this work.

the development of high performance LICs significantly depends upon the advancement of cathode materials because the cathode materials have a much lower specific capacity than anode materials.

In the LICs, the capacity of cathode materials depends upon their adsorption/desorption abilities for ions [28]. Activated carbons (ACs) with high specific surface area (SSA) and abundant porous structure are widely used as the cathode materials for LICs because of their excellent absorption/desorption performances [28–30]. However, the commonly used ACs suffer from the low conductivity and little mesoporous structure, resulting in the low power density. Except for the porous structure tuning, the advisable surface functionality is considered as the key factor in improving the performance of AC cathode materials [31]. Recently, some reports show that heteroatom doping (such as B, N doping) can increase the specific capacitance of AC materials [32–34]. Graphene structure can enhance the electrical conductivity of electrode materials and improve the power density of LICs [35–40]. Unfortunately, it is still a great challenge to develop high performance cathode materials with high energy density and power density for LICs.

Herein we report a novel graphene@hierarchical meso-/microporous carbon (G@HMMC) with advisable functional group for high performance LICs (Fig. 1a). The optimized G@HMMC shows a high SSA of  $2674.6 \text{ m}^2 \text{ g}^{-1}$ , a moderate O content of 3.99 at%, and abundant  $\text{sp}^2$  carbon. Owing to the novel structure, the optimized G@HMMC delivers a high specific capacity of  $112 \text{ mAh g}^{-1}$  for LICs. The LIC constituted by G@HMMC cathode and pre-lithiated graphite anode demonstrates an ultrahigh energy density of  $233.3 \text{ Wh kg}^{-1}$  at power density of  $450.4 \text{ W kg}^{-1}$ , and a high energy density of  $143.8 \text{ Wh kg}^{-1}$  at ultrahigh power density of

$15.7 \text{ kW kg}^{-1}$ , which is among the highest numbers reported for LICs. Thus, the G@HMMC material is one of the most promising cathode materials for LICs.

## 2. Experiments

### 2.1. Material fabrication

Graphene oxide (GO) was prepared by oxidation of graphite using modified hummers method [41]. 10 g of sucrose and 100 mg of GO were dissolved in 120 mL aqueous solution by stirring and sonication. 60 mL of sulfuric acid was added slowly to the solution and refluxed at  $120^\circ\text{C}$  for 10 h, and then the black suspension was filtered several times and dried at  $100^\circ\text{C}$  for 10 h. The obtained materials were heated at  $500^\circ\text{C}$  for 3 h. Afterwards, the obtained nanocomposite and KOH with mass ration of 1:4 were dispersed in the aqueous solution under sonication and stirring for 12 h. The obtained slurry was dried at  $100^\circ\text{C}$  for 12 h and then heated at  $800^\circ\text{C}$  for 2 h under Argon protection. Afterward, the as-prepared materials were washed with HCl solution and distilled water for several times, and then dried at  $100^\circ\text{C}$  for 10 h. The obtained products were nominated as G@HMMC800 (800 represent the activation temperature). The G@HMMC700, G@HMMC850, and G@HMMC900 samples were fabricated according to similar route mentioned above. The HMMC800 sample was fabricated without the addition of GO.

### 2.2. Material characterization

Scanning electron microscope (SEM) images were obtained

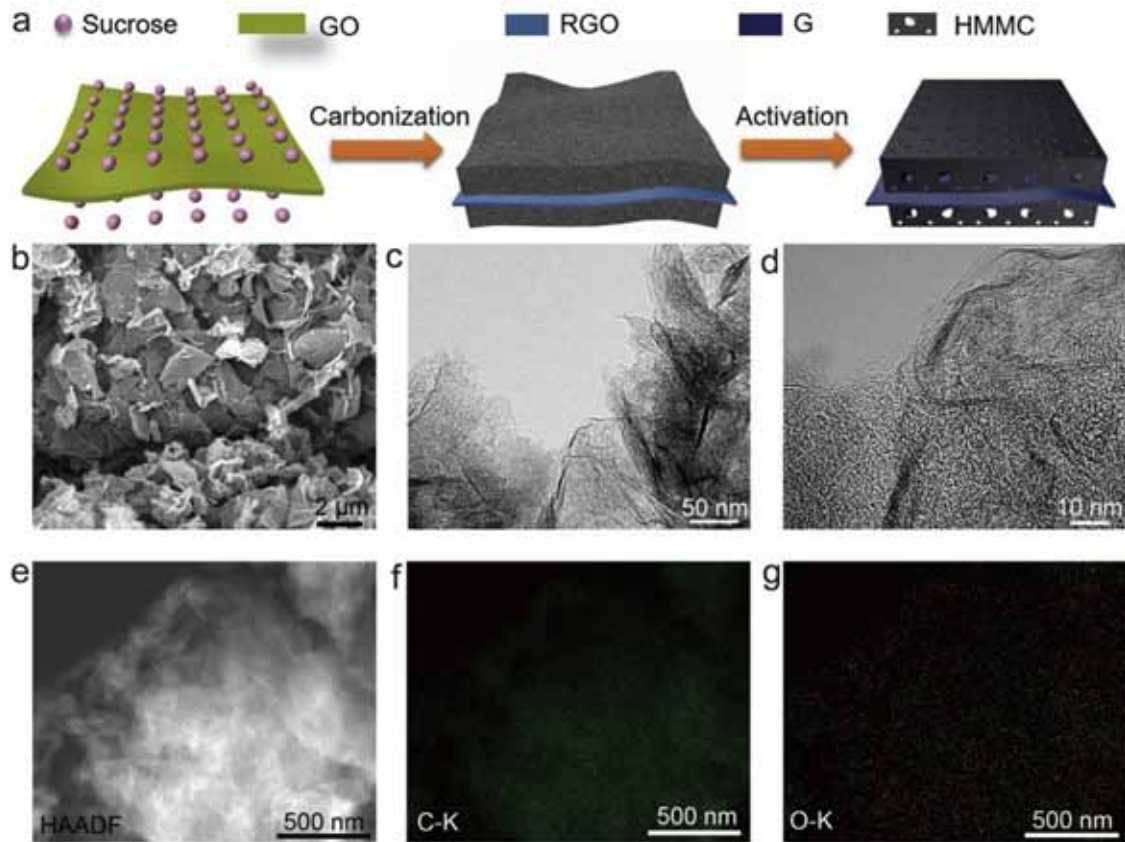


**Fig. 1.** The fabrication process of G@HMMC material (a). The SEM (b) and TEM (c,d) images of G@HMMC850 material. HAADF-TEM image (e) of G@HMMC850 and the corresponding element mappings: C (f) and O (g).

using a Nova NanoSEM 450 with a 5 kV beam voltage. Transmission electron microscope (TEM) images were measured on a Tecnai G2 F20 S-TWIN TMP instrument. N<sub>2</sub> adsorption-desorption analysis was carried out using a Quadasorb SI instrument. Raman characterization was performed on a LabRAM HR Evolution instrument with a laser wavelength of 532 nm. X-ray photoelectron spectroscopy (XPS) was examined on a Thermo Scientific ESCALab 250Xi using 200 W monochromated Al  $\text{k}\alpha$  radiation.

### 2.3. Electrochemical test

To prepare the electrodes of Li-ion capacitors (LICs) for testing, the active materials (G@HMMC, graphite) were mixed with polyvinylidene (PVDF) and conductive carbon at a ratio of 8:1:1 with N-Methyl-2-pyrrolidone (NMP) as the solvent. The cathode material (G@HMMC) was coated onto the aluminum foil and the anode material (graphite) was coated on the copper foil, respectively. The mass loading of the active materials in both cathode and anode are 4 and 2 mg, respectively. 1 M LiPF<sub>6</sub> in a mixture of ethylene carbonate, diethyl carbonate, and dimethyl carbonate (EC:DEC:DMC = 1:1:1 by volume) solution was used as the electrolyte for LICs. Lithium metal was used as the anode for half-cell of LICs. The energy density and power density were calculated based on the total mass of active materials on both cathode and anode. Electrochemical impedance spectroscopy (EIS) with a frequency range from 100 mHz to 100 kHz with an amplitude of 5 mV were performed on a Princeton PARSTAT MC 1000 multi-channel electrochemical workstation.

### 2.4. Energy and power density calculation

The capacity (mAh) was obtained directly from the instrument reading. The energy density ( $E_m$ , Wh kg<sup>-1</sup>) and power density ( $P_m$ , W kg<sup>-1</sup>) were calculated by numerically integrating the Q-V graph area during the discharge process using the formula:

$$E = \int_{t_1}^{t_2} IV dt$$

$$E_m = \frac{E}{m_a + m_b}$$

$$P_m = \frac{E_m}{\Delta t}$$

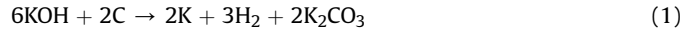
Where E (Wh) is total energy, I is the constant current density (A g<sup>-1</sup>),  $t_1$  and  $t_2$  are the start time and end time in the discharge process, V is the Voltage,  $m_a$  and  $m_b$  are the mass of cathode and anode material,  $\Delta t$  is discharge time, respectively.

## 3. Results and discussion

### 3.1. Morphology and structure characterizations

During the carbonization process, the carbon materials derived from sucrose is generated on the GO layers and assembled into sandwich-type structure, which is composed of reduced GO (RGO) and carbon nanocomposite (Fig. 1a). During the activation process, a lot of meso-/microporous structure is generated, and RGO layers are reduced to graphene by calcination at high temperature, thereby creating a three-dimensional (3D) network of G@HMMC materials. The porous structure of G@HMMC material is formed by KOH activation [42]. The predominant overall reaction

stoichiometry between KOH and carbon during chemical activation is most probably



Furthermore, the physical activation and metallic K activation are involved in KOH activation process. The typical structure of G@HMMC material is stacked by wrinkled multilayer nanosheets (Fig. 1b and S1). These nanosheets are composed of graphene sheets and porous structure, seen from the TEM images (Fig. 1c and d). Thus, the graphene structure is retained after the activation process, which is advantageous for improving the conductivity of G@HMMC materials. The element mapping (Fig. 1e–g) reveals that carbon and oxygen are uniformly distributed on the G@HMMC materials, elucidating the existing of oxygen-containing functional group. Furthermore, the SEM images of high-performance graphite anode is shown in Fig. S2.

The N<sub>2</sub> adsorption-desorption isotherms are applied to study the porous structure of HMMC and G@HMMC materials (Fig. 2a and b and Table S1). The pore distribution curves show that the HMMC and G@HMMC materials have hierarchical meso-/microporous structure (Fig. 2b). Based on all the analysis results (SEM, TEM, N<sub>2</sub> adsorption-desorption), the G@HMMC materials possess sandwich structure stacked by graphene sheets and meso-/microporous carbon. In comparison with the HMMC800, the surface area and pore volume of G@HMMC800 are found to increase slightly. The G@HMMC materials show type I curve at relative  $P/P_0 = 0$ –0.4, indicating the existing a lot of microporous structure in the G@HMMC materials. Furthermore, the hysteresis between the adsorption and desorption branches at relative  $P/P_0 = 0.4$ –0.6 can be clearly observed, demonstrating that the G@HMMC materials possess a certain amount of mesoporous structure [43–45]. The pore distribution curves show that the G@HMMC materials possess hierarchical meso-/microporous structure with peaks around 0.9, 1.6, 3, and 4 nm. The HMMC material also possesses hierarchical meso-/microporous structure with peaks around 0.9, 1.4, 1.8, and 3–4 nm, which is similar with G@HMMC materials. It is worth noting that the G@HMMC850 material has the highest surface area (2674.6 m<sup>2</sup> g<sup>-1</sup>) and the largest pore volume (1.67 cm<sup>3</sup> g<sup>-1</sup>). The carbon structure of G@HMMC materials are investigated by the Raman spectrum (Fig. 2c). With increasing of the activation temperature, the value of  $I_G/I_D$  increases in the G@HMMC materials (Fig. 2f) because of the carbonization at higher temperature. Therefore, the content of sp<sup>2</sup> hybrid carbon in the G@HMMC materials increases, which is beneficial to the conductivity of the G@HMMC materials. The X-ray photoelectron spectroscopy (XPS) is employed to further clarify the contents and types of O species in the G@HMMC materials. In the C 1s spectrum (Fig. 2d) of G@HMMC850, a small amount of C–O (286.4 eV) [46,47], C=O (288.6 eV) [48], and COO (290.9 eV) [48] group can be detected. These functional groups are advantageous to the capacity of the porous carbon because of their fast reaction with lithium and improving the wettability of the pore walls [28,32]. Deconvolution of O 1s spectrum (Fig. 2e) for G@HMMC material can be deconvoluted into C=O (531.4 eV) [49], COO (532.4 eV) [47], and C–O (533.4 eV) [47] group, which is corresponding to the C 1s spectrum. Other XPS spectrum of G@HMMC materials are shown in Figs. S3 and S4. With increasing of the activation temperature, the oxygen-containing functional groups decrease (Fig. 2f) because of the carbonization at higher temperature. The changes of pore volume, the value of  $I_G/I_D$ , and oxygen-containing functional group on the surface of G@HMMC materials with different activation temperature are summarized in Fig. 2f. These parameters play important roles in the electrochemical performance of the G@HMMC materials.

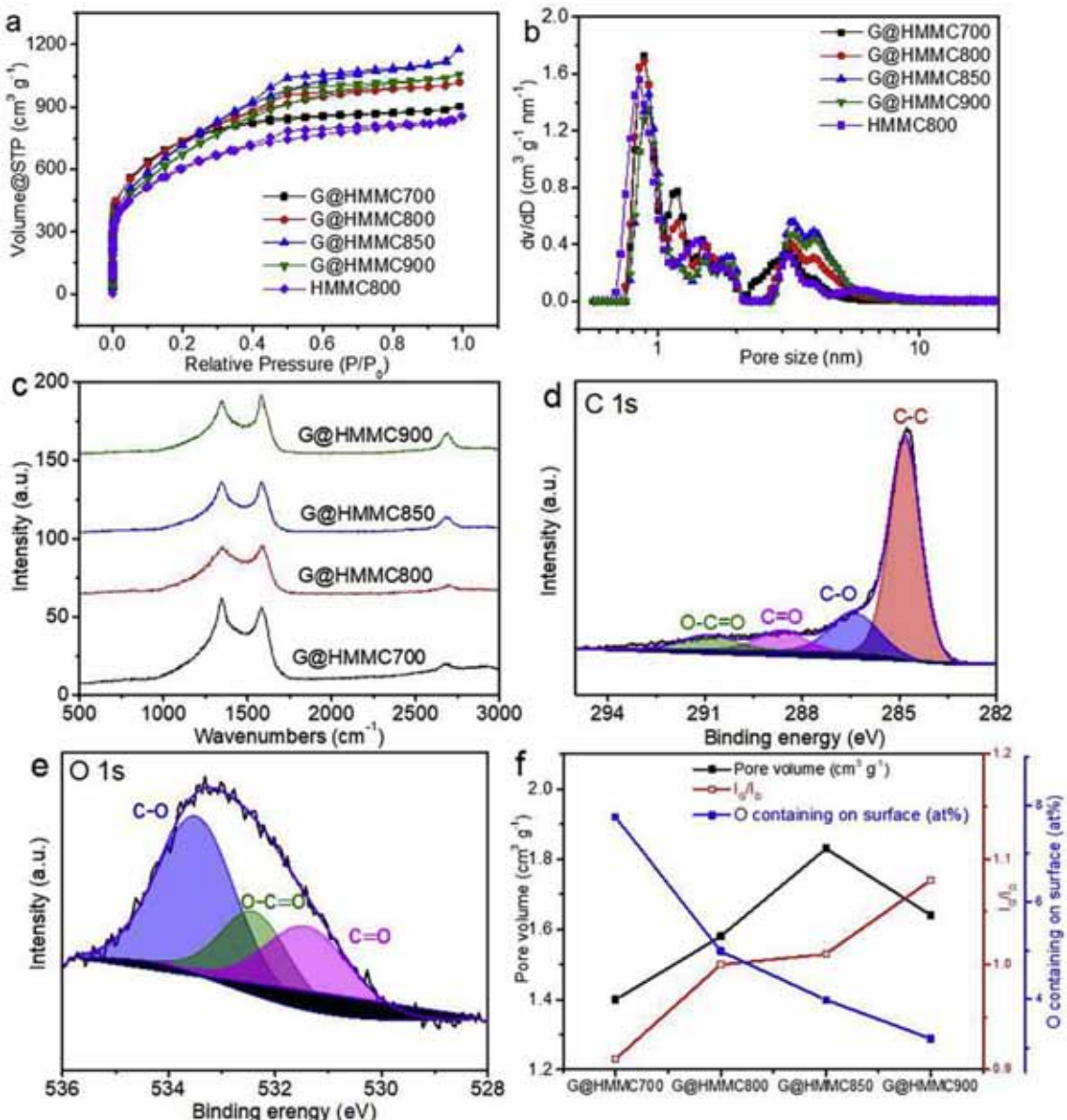


**Fig. 2.** The  $N_2$  adsorption/desorption (a) and pore distribution curves (b) of HMMC and G@HMMC materials. Raman spectra of G@HMMC materials. C 1s (d) and O 1s (e) XPS spectra of G@HMMC850. The pore volume, O containing on surface, and  $I_G/I_D$  values (f) of G@HMMC materials.

### 3.2. Electrochemical performance

To evaluated the electrochemical performance of the G@HMMC materials, half-cell tests were carried out using coin cells with Li foil as counter electrodes. Type charge/discharge curves of the G@HMMC materials in the potential range of 2–4.5 V are shown in Fig. 3a. At current density of  $1 A g^{-1}$ , the G@HMMC700, HMMC800, G@HMMC800, G@HMMC850, and G@HMMC900 material show discharge capacity of 101.8, 98.0, 106.9, 103.5, and  $73.2 mAh g^{-1}$ , and deliver capacity of 87.4, 86.2, 98.5, 102.5, and  $75.1 mAh g^{-1}$  after 300 cycles, respectively (Fig. 3b). The rate performance of G@HMMC materials improve markedly with increasing of the activation temperature (Fig. 3c). Fig. 3d shows the Nyquist plots of HMMC800 and G@HMMC materials. These curves are fitted by an electric equivalent circuit model (Fig. S5). The value of  $R_{e}$  for HMMC and G@HMMC materials is approximate. The charge transfer resistance of G@HMMC materials decreases with the increasing of

activation temperature because of the improved conductivity of G@HMMC materials at higher activation temperature. It is worth noting that the introduction of graphene structure can significantly reduce the charge transfer resistance of HMMC materials, thereby improving the rate performance and cycling performance of HMMC material. The G@HMMC materials show higher capacity than the graphene material without activation (Fig. S6). Thus, the HMMC structure can improve the capacity of carbon materials. The G@HMMC800 material possesses the highest discharge capacity, while its rate performance and cycling performance is inferior to G@HMMC850 and G@HMMC900. The G@HMMC900 material possesses the best cycling performance and rate performance, while its capacity is lower than other materials. Consequently, the G@HMMC850 material possesses the best electrochemical performance.

To investigate the electrochemical performance of G@HMMC materials in LIC, G@HMMC850 is selected as the cathode material

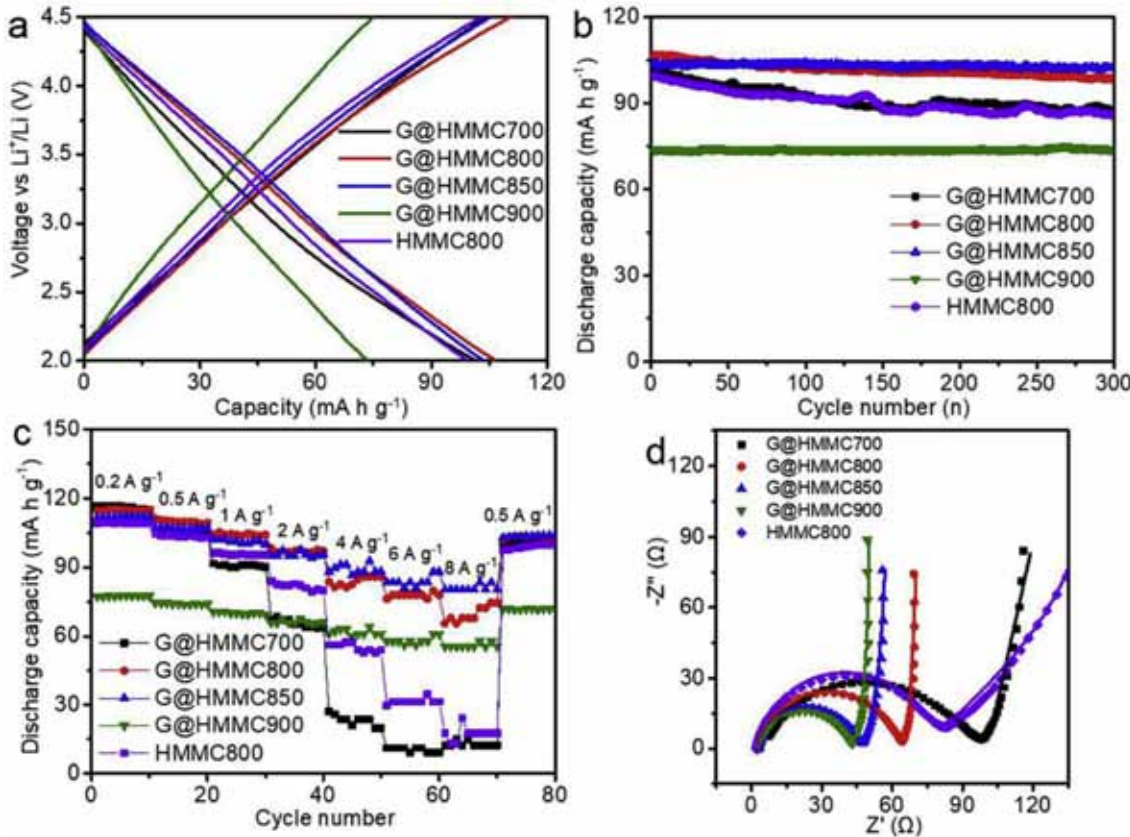


**Fig. 3.** The charge/discharge curves (a) and cycling stability (b) of HMMC800 and G@HMMC materials. The rate performances (c) and Nyquist plots (d) of HMMC800 and G@HMMC materials.

and pre-lithiated graphite is selected as the anode material. The discharge/charge curves and cycling performance of G@HMMC850 at potential range of 2–4.6 V are shown in Fig. S7. The high-performance graphite exhibits excellent electrochemical performance (Fig. S8). As shown in Fig. 4a, the G@HMMC based LIC delivers a capacity of 112 mAh g<sup>-1</sup> at a current density of 0.2 A g<sup>-1</sup> and a capacity of 73.3 mAh g<sup>-1</sup> at a current density of 8.0 A g<sup>-1</sup>, confirming the remarkable rate performance of the G@HMMC based LIC. It is worth noting that LIC composed of G@HMMC850 cathode and lithiated graphite anode can achieve an ultrahigh energy of 233.3 Wh kg<sup>-1</sup> at a power density of 450 W kg<sup>-1</sup> (Fig. 4c), which is the highest value for hybrid capacitor that ever reported before [24,32,34,39]. Furthermore, it still can retain 143.8 Wh kg<sup>-1</sup> at an ultrahigh power density of 15.7 kW kg<sup>-1</sup>. The G@HMMC based LIC demonstrates an excellent cycling stability (90.6% capacity retention after 3000 cycles at a current density of 1 A g<sup>-1</sup>) and a good Coulombic efficiency (about 98–99%) during the long cycling (Fig. 4d). Furthermore, the G@HMMC based LIC exhibits outstanding cycling stability for 10000 cycles (Fig. S9). The high energy density and power capability of the G@HMMC material based LIC are superior to previously LICs, such as MnO<sub>2</sub>/GNS//HNC [38], active carbon//Si-C [27], activated polyaniline-derived carbon//VN-RGO [26], and GNS//GNS-TiO<sub>2</sub> [36]. In addition, the G@HMMC material based LIC shows excellent performance in aqueous electrolyte (Fig. S10).

### 3.3. Discussion

In the LICs, the capacity of cathode material is depending on their adsorption ability for anion. Therefore, the structure and

surface functional group play crucial roles in the performance of cathode material for LICs. The graphene structure can improve the rate performance and cycling stability of cathode material by reducing the charge transfer resistance. With the increasing of activation temperature, the oxygen-containing groups on surface of G@HMMC materials decrease, and the sp<sup>2</sup> hybrid carbon content increases in the G@HMMC materials, thereby reducing the charge transfer resistances of G@HMMC materials. Consequently, the rate performance and cycling stability of G@HMMC materials are improved with the activation temperature. The G@HMMC850 material possesses larger surface area and higher pore volume than the G@HMMC800 material, while the G@HMMC800 material has higher discharge capacity in the LIC. The most likely reason is that the G@HMMC800 material has higher oxygen-containing groups than G@HMMC850 material. The oxygen-containing groups including C—O, C=O, and COO may increase the ions adsorption capacity and improve the wettability of the pore walls of carbon materials, which is similar to the previous reports [33,50,51]. Therefore, the G@HMMC900 material with little oxygen-containing group has lower capacity than other G@HMMC materials. In this ingenious designed strategy, the hierarchical meso-/microporous structure provides abundant adsorption sites for the PF<sub>6</sub><sup>-</sup> ions, the abundant sp<sup>2</sup> type hybrid carbon enhances the conductivity of G@HMMC materials, and the appropriate oxygen-containing groups improve the adsorption capacity of the G@HMMC materials. Consequently, the rational designed G@HMMC850 cathode and pre-lithiated graphite anode possesses high discharge capacity, good cycling stability, and excellent rate performance for LICs. This design strategy provides a promising route for LICs with high energy density at high power density.

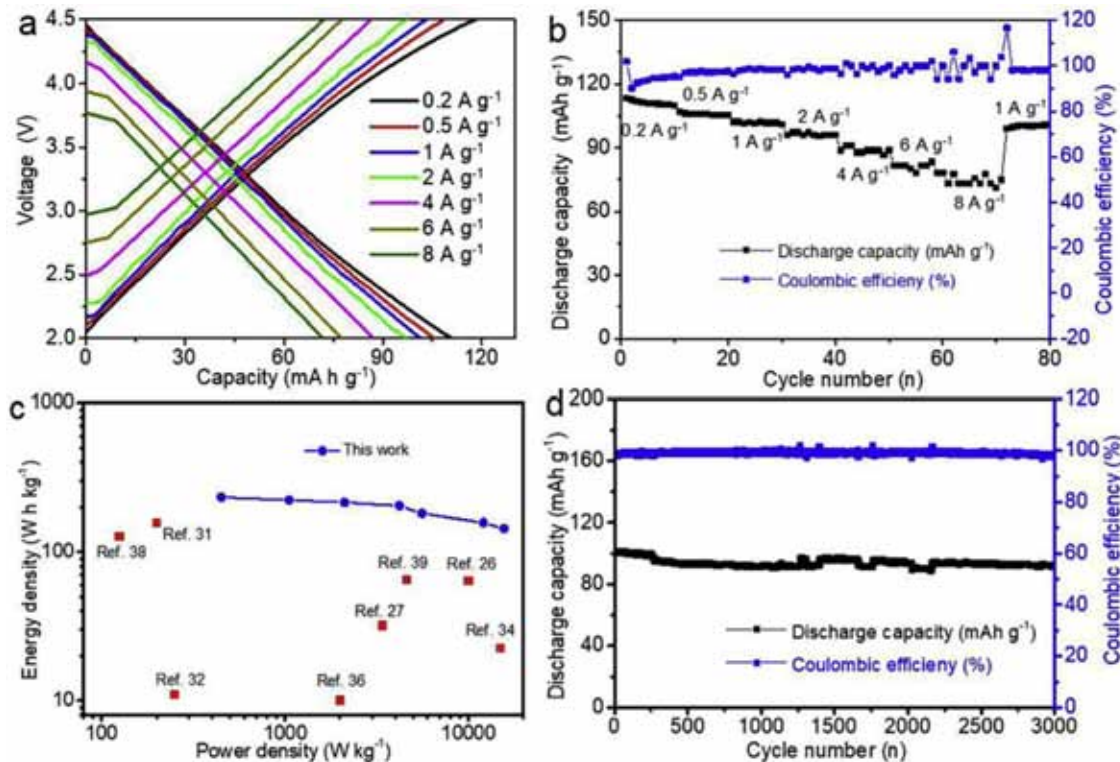


**Fig. 4.** Full cell performance. The discharge/charge curves (a), rate performance (b), and long cycling performance (d) of LIC composed of G@HMMC850 and pre-lithiated graphite. Ragone plot (c) of the present LIC compared with previously reports.

#### 4. Conclusion

In summary, a series of G@HMMC materials with hierarchical meso-/microporous structure, graphene structure, and oxygen-containing groups are designed for high performance LICs. The hierarchical meso-/microporous structure provides abundant adsorption active sites, the  $sp^2$  type carbon enhances the electronic transmission performance, and the oxygen-containing groups improve the specific capacity. Therefore, the ingenious designed LICs composed of optimized G@HMMC cathode and pre-lithiated graphite anode exhibit high energy densities of 233.3–143.8 Wh kg<sup>-1</sup> at power densities from 450.4 to 15686 W kg<sup>-1</sup>, which are among the highest numbers reported for LICs. In addition, the G@HMMC850 material has good cycling performance (90.6% capacity retention after 3000 cycles) for LIC. Consequently, the G@HMMC material is one of the most promising cathode materials for LICs. This simultaneous manipulation of hierarchical meso-/microporous structure and graphene nanocomposite with reasonable oxygen-containing groups offers new opportunities for the high-performance electrode material.

#### Acknowledgements

This work is supported by the Beijing Natural Science Foundation (Nos. 2182014), and the National Natural Science Foundation of China (NSFC Nos. 21703010, 51503005 and 21274006), National Key R&D Project from Minister of Science and Technology (2016YFA0202702, 2016YFA0202703, and 2016YFA0202704), and the Programs for Beijing Science and Technology Leading Talent (Grant no. Z161100004916168), and the Beijing Hundred, Thousand and Ten Thousand Talent Project (110403000402), and the “Thousands Talents” Program for Pioneer Researcher and His Innovation Team, China.

#### Appendix A. Supplementary data

Supplementary data related to this article can be found at <https://doi.org/10.1016/j.electacta.2018.05.147>.

#### References

- P. Jezowski, K. Fic, O. Crosnier, T. Brousse, F. Beguin, Use of sacrificial lithium nickel oxide for loading graphitic anode in Li-ion capacitors, *Electrochim. Acta* 206 (2016) 440–445.
- X.Z. Sun, X. Zhang, W.J. Liu, K. Wang, C. Li, Z. Li, Y.W. Ma, Electrochemical performances and capacity fading behaviors of activated carbon/hard carbon lithium ion capacitor, *Electrochim. Acta* 235 (2017) 158–166.
- X.Q. Han, P.X. Han, J.H. Yao, S. Zhang, X.Y. Cao, J.W. Xiong, J.N. Zhang, G.L. Cui, Nitrogen-doped carbonized polyimide microsphere as a novel anode material for high performance lithium ion capacitors, *Electrochim. Acta* 196 (2016) 603–610.
- N.-W. Li, Y.-X. Yin, S. Xin, J.-Y. Li, Y.-G. Guo, Methods for the stabilization of nanostructured electrode materials for advanced rechargeable batteries, *Small Methods* 1 (2017), 1700094.
- Q. Deng, P. Huang, W.X. Zhou, Q. Ma, N. Zhou, H. Xie, W. Ling, C.J. Zhou, Y.X. Yin, X.W. Wu, X.Y. Lu, Y.G. Guo, A high-performance composite electrode for vanadium redox flow batteries, *Adv. Energy Mater.* 7 (2017), 1700461.
- V. Aravindan, J. Gnanaraj, Y.S. Lee, S. Madhavi, Insertion-type electrodes for nonaqueous Li-ion capacitors, *Chem. Rev.* 114 (2014) 11619–11635.
- D.P. Dubal, O. Ayyad, V. Ruiz, P. Gomez-Romero, Hybrid energy storage: the merging of battery and supercapacitor chemistries, *Chem. Soc. Rev.* 44 (2015) 1777–1790.
- J. Xu, Z.Q. Tan, W.C. Zeng, G.X. Chen, S.L. Wu, Y. Zhao, K. Ni, Z.C. Tao, M. Ikram, H.X. Ji, Y.W. Zhu, A hierarchical carbon derived from sponge-templated activation of graphene oxide for high-performance supercapacitor electrodes, *Adv. Mater.* 28 (2016) 5222–5228.
- J.F. Chen, Y.L. Han, X.H. Kong, X.Z. Deng, H.J. Park, Y.L. Guo, S. Jin, Z.K. Qi, Z. Lee, Z.H. Qiao, R.S. Ruoff, H.X. Ji, The origin of improved electrical double-layer capacitance by inclusion of topological defects and dopants in graphene for supercapacitors, *Angew. Chem. Int. Ed.* 55 (2016) 13822–13827.
- Y.R. Jiang, X. Zheng, X.Q. Yan, Y. Li, X. Zhao, Y. Zhang, 3D architecture of a graphene/CoMoO<sub>4</sub> composite for asymmetric supercapacitors usable at various temperatures, *J. Colloid Interface Sci.* 493 (2017) 42–50.
- Y. Li, Z. Kang, X.Q. Yan, S.Y. Cao, M.H. Li, Y.C. Liu, S. Liu, Y.H. Sun, X. Zheng, Y. Zhang, A facile method for the preparation of three-dimensional CNT

- sponge and a nanoscale engineering design for high performance fiber-shaped asymmetric supercapacitors, *J. Mater. Chem. A* 5 (2017) 22559–22567.
- [12] Y. Li, X.Q. Yan, X. Zheng, H.N. Si, M.H. Li, Y.C. Liu, Y.H. Sun, Y.R. Jiang, Y. Zhang, Fiber-shaped asymmetric supercapacitors with ultrahigh energy density for flexible/wearable energy storage, *J. Mater. Chem. A* 4 (2016) 17704–17710.
- [13] Q. Zhang, Q.J. Liang, Q.L. Liao, F. Yi, X. Zheng, M.Y. Ma, F.F. Gao, Y. Zhang, Service behavior of multifunctional triboelectric nanogenerators, *Adv. Mater.* 29 (2017), 1606703.
- [14] X. Zheng, X.Q. Yan, Y.H. Sun, Y. Li, M.H. Li, G.J. Zhang, Y. Zhang, Band alignment engineering for high-energy-density solid-state asymmetric supercapacitors with TiO<sub>2</sub> insertion at the ZnO/Ni(OH)<sub>2</sub> interface, *J. Mater. Chem. A* 4 (2016) 17981–17987.
- [15] X. Yu, J. Deng, C. Zhan, R. Lv, Z.-H. Huang, F. Kang, A high-power lithium-ion hybrid electrochemical capacitor based on citrate-derived electrodes, *Electrochim. Acta* 228 (2017) 76–81.
- [16] J. Zhang, X.F. Liu, J. Wang, J.L. Shi, Z.Q. Shi, Different types of pre-lithiated hard carbon as negative electrode material for lithium-ion capacitors, *Electrochim. Acta* 187 (2016) 134–142.
- [17] K. Naoi, S. Ishimoto, J. Miyamoto, W. Naoi, Second generation 'nanohybrid supercapacitor': Evolution of capacitive energy storage devices, *Energy Environ. Sci.* 5 (2012) 9363–9373.
- [18] M. Sevilla, R. Mokaya, Energy storage applications of activated carbons: supercapacitors and hydrogen storage, *Energy Environ. Sci.* 7 (2014) 1250–1280.
- [19] H. Wang, C. Zhu, D. Chao, Q. Yan, H.J. Fan, Nonaqueous hybrid lithium-ion and sodium-ion capacitors, *Adv. Mater.* 29 (2017), 1702093.
- [20] P.X. Han, X.Q. Han, J.H. Yao, L.X. Zhang, X.Y. Cao, C.S. Huang, G.L. Cui, High energy density sodium-ion capacitors through co-intercalation mechanism in diglyme-based electrolyte system, *J. Power Sources* 297 (2015) 457–463.
- [21] C.h. Lee, C. Jung, Enhancement of Li<sup>+</sup> ions mobility on activated carbon electrode for lithium ion capacitor, *Electrochim. Acta* 232 (2017) 596–600.
- [22] E. Lim, C. Jo, H. Kim, M.-H. Kim, Y. Mun, J. Chun, Y. Ye, J. Hwang, K.-S. Ha, K.C. Roh, K. Kang, S. Yoon, J. Lee, Facile synthesis of Nb<sub>2</sub>O<sub>5</sub>@Carbon core–shell nanocrystals with controlled crystalline structure for high-power anodes in hybrid supercapacitors, *ACS Nano* 9 (2015) 7497–7505.
- [23] E. Lim, H. Kim, C. Jo, J. Chun, K. Ku, S. Kim, H.I. Lee, I.-S. Nam, S. Yoon, K. Kang, J. Lee, Advanced hybrid supercapacitor based on a mesoporous niobium pentoxide/carbon as high-performance anode, *ACS Nano* 8 (2014) 8968–8978.
- [24] C. Liu, C. Zhang, H. Fu, X. Nan, G. Cao, Exploiting high-performance anode through tuning the character of chemical bonds for Li-Ion batteries and capacitors, *Adv. Energy Mater.* 7 (2017), 1601127.
- [25] H.W. Wang, Y. Zhang, H.X. Ang, Y.Q. Zhang, H.T. Tan, Y.F. Zhang, Y.Y. Guo, J.B. Franklin, X.L. Wu, M. Srinivasan, H.J. Fan, Q.Y. Yan, A high-energy lithium-ion capacitor by integration of a 3D interconnected titanium carbide nanoparticle chain anode with a pyridine-derived porous nitrogen-doped carbon cathode, *Adv. Funct. Mater.* 26 (2016) 3082–3093.
- [26] R. Wang, J. Lang, P. Zhang, Z. Lin, X. Yan, Fast and large lithium storage in 3D porous VN nanowires–graphene composite as a superior anode toward high-performance hybrid supercapacitors, *Adv. Funct. Mater.* 25 (2015) 2270–2278.
- [27] R. Yi, S.R. Chen, J.X. Song, M.L. Gordin, A. Manivannan, D.H. Wang, High-performance hybrid supercapacitor enabled by a high-rate Si-based anode, *Adv. Funct. Mater.* 24 (2014) 7433–7439.
- [28] J. Ding, H.L. Wang, Z. Li, K. Cui, D. Karpuzov, X.H. Tan, A. Kohandehghan, D. Mitlin, Peanut shell hybrid sodium ion capacitor with extreme energy-power rivals lithium ion capacitors, *Energy Environ. Sci.* 8 (2015) 941–955.
- [29] Y.F. Ma, H.C. Chang, M. Zhang, Y.S. Chen, Graphene-based materials for lithium-ion hybrid supercapacitors, *Adv. Mater.* 27 (2015) 5296–5308.
- [30] S.R. Sivakkumar, A.G. Pandolfo, Evaluation of lithium-ion capacitors assembled with pre-lithiated graphite anode and activated carbon cathode, *Electrochim. Acta* 65 (2012) 280–287.
- [31] W.S.V. Lee, E. Peng, M. Li, X.L. Huang, J.M. Xue, Rational design of stable 4 V lithium ion capacitor, *Nano Energy* 27 (2016) 202–212.
- [32] L.F. Chen, Y. Lu, L. Yu, X.W. Lou, Designed formation of hollow particle-based nitrogen-doped carbon nanofibers for high-performance supercapacitors, *Energy Environ. Sci.* 10 (2017) 1777–1783.
- [33] B. Li, F. Dai, Q.F. Xiao, L. Yang, J.M. Shen, C.M. Zhang, M. Cai, Nitrogen-doped activated carbon for a high energy hybrid supercapacitor, *Energy Environ. Sci.* 9 (2016) 102–106.
- [34] Q. Xia, H. Yang, M. Wang, M. Yang, Q. Guo, L. Wan, H. Xia, Y. Yu, High energy and high power lithium-ion capacitors based on boron and nitrogen dual-doped 3D carbon nanofibers as both cathode and anode, *Adv. Energy Mater.* (2017), 1701336.
- [35] S.H. Li, J.W. Chen, M.Q. Cui, G.F. Cai, J.X. Wang, P. Cui, X.F. Gong, P.S. Lee, A high-performance lithium-ion capacitor based on 2D nanosheet materials, *Small* 13 (2017), 1602893.
- [36] F. Wang, C. Wang, Y. Zhao, Z. Liu, Z. Chang, L. Fu, Y. Zhu, Y. Wu, D. Zhao, A Quasi-solid-state Li-Ion capacitor based on porous TiO<sub>2</sub> hollow microspheres wrapped with graphene nanosheets, *Small* 12 (2016) 6207–6213.
- [37] H. Wang, C. Guan, X. Wang, H.J. Fan, A high energy and power Li-Ion capacitor based on a TiO<sub>2</sub> nanobelト array anode and a graphene hydrogel cathode, *Small* 11 (2015) 1470–1477.
- [38] M. Yang, Y.R. Zhong, J.J. Ren, X.L. Zhou, J.P. Wei, Z. Zhou, Fabrication of high-power Li-Ion hybrid supercapacitors by enhancing the exterior surface charge storage, *Adv. Energy Mater.* 5 (2015), 1500550.
- [39] F. Zhang, T.F. Zhang, X. Yang, L. Zhang, K. Leng, Y. Huang, Y.S. Chen, A high-performance supercapacitor-battery hybrid energy storage device based on graphene-enhanced electrode materials with ultrahigh energy density, *Energy Environ. Sci.* 6 (2013) 1623–1632.
- [40] L. Zhao, H. Li, M. Li, S. Xu, C. Li, C. Qu, L. Zhang, B. Yang, Lithium-ion storage capacitors achieved by CVD graphene/TaC/Ta-wires and carbon hollow spheres, *Appl. Energy* 162 (2016) 197–206.
- [41] N.W. Li, M.B. Zheng, H.L. Lu, Z.B. Hu, C.F. Shen, X.F. Chang, G.B. Ji, J.M. Cao, Y. Shi, High-rate lithium-sulfur batteries promoted by reduced graphene oxide coating, *Chem. Commun.* 48 (2012) 4106–4108.
- [42] J.C. Wang, S. Kaskel, KOH activation of carbon-based materials for energy storage, *J. Mater. Chem.* 22 (2012) 23710–23725.
- [43] N.W. Li, Y.X. Yin, Y.G. Guo, Three-dimensional sandwich-type graphene@microporous carbon architecture for lithium-sulfur batteries, *RSC Adv.* 6 (2016) 617–622.
- [44] S.T. Zhang, M.B. Zheng, Z.X. Lin, R. Zang, Q.L. Huang, H.G. Xue, J.M. Cao, H. Pang, Mango stone-derived activated carbon with high sulfur loading as a cathode material for lithium-sulfur batteries, *RSC Adv.* 6 (2016) 39918–39925.
- [45] N.W. Li, M.B. Zheng, S.Q. Feng, H.L. Lu, B. Zhao, J.F. Zheng, S.T. Zhang, G.B. Ji, J.M. Cao, Fabrication of hierarchical macroporous/mesoporous carbons via the dual-template method, and the restriction effect of hard template on shrinkage of mesoporous polymers, *J. Phys. Chem. C* 117 (2013) 8784–8792.
- [46] N.W. Li, Y.X. Yin, C.P. Yang, Y.G. Guo, An artificial solid electrolyte interphase layer for stable lithium metal anodes, *Adv. Mater.* 28 (2016) 1853–1858.
- [47] C. Mattevi, G. Eda, S. Agnoli, S. Miller, K.A. Mkhoyan, O. Celik, D. Mastrogianni, G. Granozzi, E. Garfunkel, M. Chhowalla, Evolution of electrical, chemical, and structural properties of transparent and conducting chemically derived graphene thin films, *Adv. Funct. Mater.* 19 (2009) 2577–2583.
- [48] N.-W. Li, Y.-X. Yin, J.-Y. Li, C.-H. Zhang, Y.-G. Guo, Passivation of lithium metal anode via hybrid ionic liquid electrolyte toward stable Li plating/stripping, *Adv. Sci.* 3 (2016), 1600400.
- [49] M. Seredych, A.V. Tamashausky, T.J. Bandosz, Graphite oxides obtained from porous graphite: the role of surface chemistry and texture in ammonia retention at ambient conditions, *Adv. Funct. Mater.* 20 (2010) 1670–1679.
- [50] Z. Li, Z. Xu, X. Tan, H. Wang, C.M.B. Holt, T. Stephenson, B.C. Olsen, D. Mitlin, Mesoporous nitrogen-rich carbons derived from protein for ultra-high capacity battery anodes and supercapacitors, *Energy Environ. Sci.* 6 (2013) 871–878.
- [51] B. Xu, S. Yue, Z. Sui, X. Zhang, S. Hou, G. Cao, Y. Yang, What is the choice for supercapacitors: graphene or graphene oxide? *Energy Environ. Sci.* 4 (2011) 2826–2830.